THE JOURNAL OF PHYSICAL CHEMISTRY B

Article

pubs.acs.org/JPCB

Scaling Relations and Optimization of Excitonic Energy Transfer Rates between One-Dimensional Molecular Aggregates

Chern Chuang,[†] Jasper Knoester,[‡] and Jianshu Cao*,[†]

[†]Department of Chemistry, Massachusetts Institute of Technology, Cambridge, Massachusetts 02139, United States

[‡]Zernike Institute for Advanced Materials, University of Groningen, Nijenborgh 4, AG Groningen 9747, The Netherlands

ABSTRACT: We theoretically study the distance, chain length, and temperature dependence of the electronic couplings as well as the excitonic energy transfer rates between one-dimensional (1D) chromophore aggregates. In addition to the well-known geometry dependent factor that leads to the deviation from Förster's classic R_{DA}^{-6} scaling on the donor−acceptor separation, nonmonotonic dependence on aggregate size and the breakdown of far-field dipole selection rules are also investigated in detail and compared to prior calculations. Our analysis provides a simple, unifying framework to bridge the results of the ground state electronic couplings at low temperatures and those from the classical rate-summation at high temperatures. At low temperatures and in the near-field limit, the exciton transfer integral scales as R_{DA}^{-1}, in analogy to that of electric monopoles. For the case of aligned 1D J-aggregates, we predict a maximal excitonic energy transfer rate at temperatures on the order of the intra-aggregate coupling strength.

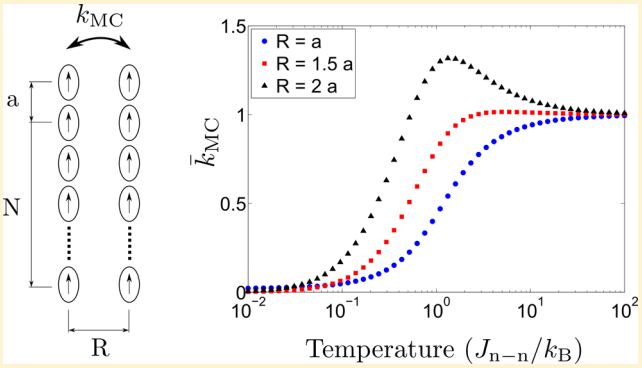

INTRODUCTION

More than half a century after its development, the theory of Förster resonance energy transfer (FRET)[1] has received increased attention in the field of condensed matter sciences owing to technological advances to manipulate molecules on the nano scale and to decipher the molecular details of important biological systems. The FRET theory has found wide applications in the study of conformational dynamics and excitation energy transfer (EET) of polymers, be it biological systems like DNA and proteins or artificial ones with promising physical properties such as conjugated polymers.[2] The popularity and success of the FRET theory can be ascribed to an insightful approximation made by Förster: treating the Coulomb interaction between the donor−acceptor pair only to the second order, which can then be expressed in terms of the respective transition dipole moments. By incorporating the square of the donor (acceptor) transition dipole into the expression of the donor emission (acceptor absorption) spectrum, the FRET rate is conveniently written down as a combination of experimental measurables, in particular the overlap between the donor's emission spectrum and the acceptor's absorption spectrum. Furthermore, it gives rise to the classic R_{DA}^{-6} dependence on the donor−acceptor separation R_{DA} of the EET rate, which is a manifestation of the dipolar interaction as well. As a consequence, variations of the measured FRET rate (in time) imply variations of the chromophoric donor−acceptor separation to the sixth power. See some of the recent reviews for more in depth discussions.[2−6]

However, the validity of Förster's original theory is questionable in numerous circumstances. Sumi[7] was the first to point out that in multichromophoric (MC) systems, where the exciton may be delocalized over several chromophores, considerable contributions to exciton transport arise from optically dark states. While this situation is typical in the light-harvesting apparatus of photosynthetic bacteria and green plants, as well as synthetic molecular systems such as organic photovoltaic systems and the low-dimensional aggregates formed by amphiphilic cyanine dyes,[8] the FRET theory can critically underestimate the EET rate.[2,7] The essential point is that in many cases the physical dimension of aggregates is comparable to or exceeds the separation R_{DA}. This leads to the failure of the dipole approximation. Recently, we developed numerical and analytical methods to systematically evaluate EET rates in multichromophoric systems. For the current study, we will adopt physical approximations to establish scaling laws and refer readers to a series of papers for details of rate calculations.[9]

In a recent work by Emelianova et al., the authors considered the energy diffusion in organic molecular crystals.[10] Due to the reduced energetic disorder in these materials, 2D-delocalized excitons were proposed as primary agents for EET, where the reduced dimensionality results from the high anisotropy in

Special Issue: James L. Skinner Festschrift

Received: December 19, 2013
Revised: March 3, 2014
Published: March 19, 2014

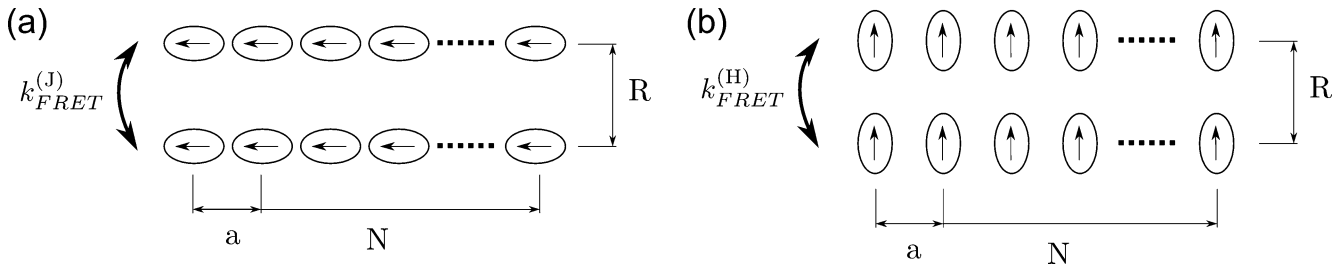

Figure 1. System geometries examined in this study. (a) Energy transfer between two linear aggregates with all the transition dipole moments parallel to the axis of aggregation. This is referred to as a perfect J-aggregate. (b) Parallel linear aggregates with transition dipole moments perpendicular to the direction of aggregation and lying in the plane of superaggregate structure. This is referred to as a perfect H-aggregate. In both cases R is the separation between the aggregates, a is the intra-aggregate spacing between chromophores, and N is the number of chromophores in each aggregate.

electronic couplings: strong couplings in the *ab* plane, while couplings between layers are considerably weaker. They found a peculiar temperature dependence of the interlayer EET rate, namely for the J-aggregate configuration the rate is peaked at intermediate temperatures as opposed to the monotonic behavior for the H-aggregate case. This can be attributed to the contribution from the optically forbidden states that are close to the bottom of the exciton band, which also leads to the deviation from the R^{-4} scaling of the interlayer coupling obtained with classical theory.[11] The peaking of the EET rate at an optimal temperature originates from the maximal overlap between the thermal population distribution of exciton states and the EET rates among individual donor−acceptor states.[12] This is one of the many aspects of achieving efficient and robust EET through optimal system−bath interactions,[12−14] which are often found in natural light-harvesting systems and have profound implications on improving current solar energy industry.

The present work concerns a similar scheme with a change in dimensionality. We look at the EET between close-lying 1D chromophore aggregates (see the schematics in Figure 1).[15] This is in part motivated by the technological advancement of manufacturing devices containing aligned conjugated polymers[16] as well as growing single-crystalline organic thin films.[17] In such cases, the EET in the direction perpendicular to the stronger-coupled dimension becomes a central issue in controlling the anisotropy of the devices. For example, anisotropy of exciton transport has been observed in phthalocyanine and porphyrin derivatives thin films.[18] Clear indication of faster exciton diffusion within 1D columnar aggregate structures and slower interstack exciton transfer was characterized through analyzing the fluorescence anisotropy decay of the systems.[19−21] On the other hand, there are several previous studies on the photophysics of conjugated oligomers/polymers,[22−25] where nonmonotonic dependence on chain length and deviation from the R^{-6} scaling were observed. It should be noted that analytical results for this system have been obtained in the zero-temperature limit,[26,27] which are valid for conjugated polymers/oligomers since the gaps between exciton levels are much larger than the thermal energy in these systems.

Here we extend the analysis of Emlianova et al. to the EET in these 1D systems and obtain closed expressions for the transfer integrals as functions of the quasi-momenta of the 1D excitons. We first discuss the classical results obtained with the sum-over-rates approach. The corresponding quantum results, which account for the electronic couplings among all states of the donor and the acceptor aggregates, are presented thereafter. The proper recovery of the classical expression is presented and discussed, as wells as its use to explain prior observations with emphasis on the scaling relations and temperature dependence of EET rate.

CLASSICAL FRET: SUM OVER RATES

Let us first consider the classical FRET rates between linear aggregates consisting of identical chromophores, whose results shall serve as references in the following sections. Treating all the chromophores as two level systems, the coupling Hamiltonian is written as

$$H_{\mathrm{DA}} = \sum_{m=1}^{N_{\mathrm{D}}} \sum_{n=1}^{N_{\mathrm{A}}} J_{mn} |m\rangle\langle n| \tag{1}$$

where for notational simplicity m (n) always refers to the site label of the donor (acceptor) aggregate, and $|x\rangle$ ($x = m,n$) represents the state where the xth site is in its excited state and all others being in the ground state. N_{D} and N_{A} are the number of monomers in the donor and the acceptor aggregates, respectively. The couplings J_{mn} will be approximated by dipole−dipole interaction

$$J_{mn} = \frac{\vec{\mu}_m \cdot \vec{\mu}_n}{r_{mn}^3} - 3\frac{(\vec{\mu}_m \cdot \vec{r}_{mn})(\vec{\mu}_n \cdot \vec{r}_{mn})}{r_{mn}^5} \tag{2}$$

with $\vec{\mu}_m$ and $\vec{\mu}_n$ being the transition dipole moments and r_{mn} the distance between sites m and n of the respective aggregates. The magnitudes of the dipole moments are set to unity. The FRET rate between the donor and the acceptor aggregates is written down as a summation over the individual rates of all donor−acceptor pairs, regardless of the intra-aggregate couplings, as follows[2]

$$k_{\mathrm{C}} = \frac{2\pi}{\hbar}\frac{1}{N_{\mathrm{D}}} \sum_{m=1}^{N_{\mathrm{D}}} \sum_{n=1}^{N_{\mathrm{A}}} J_{mn}^2 S_{mn} \tag{3}$$

Here S_{mn} denotes the overlap integral between the lineshapes of monomer m and n.[28] The above expression indicates that no coherence exists between any two sites, and at high temperatures the quantum expression discussed in the next section should reduce to this classical one. In addition, treating S_{mn} as constants, we focus our study essentially on the inter-aggregate couplings J_{mn}. The latter has the unit of energy squared, where we have set $\mu^2/4\pi\varepsilon_0$ to unity and left only the distance dependence explicit. To get the physical EET rate one has to return to eq 3 and pick up suitable estimations of the above-mentioned parameters as in ref 10 Also, the N_{D}^{-1} factor

dx.doi.org/10.1021/jp4124502 | J. Phys. Chem. B 2014, 118, 7827−7834

corresponds to an average over all donor chromophores, accounting for an equal distribution of the initial excitation.

In this study we will consider a convenient setup of system geometries, as shown in Figure 1. Two extreme cases are considered, in (a) the two linear chromophoric aggregates are aligned in parallel with all the transition dipole moments pointing along the axis of aggregation, while in (b) the dipoles are perpendicular to the axis in the plane of paper. We refer to the former as a perfect J-aggregate and the latter as a perfect H-aggregate for obvious reasons. For simplicity, we set $N_D = N_A = N$. Discussions on a more general scheme are presented in the Appendix. In the following, R denotes the separation between the aggregates. In the continuum limit ($R \gg a$, where a is the intra-aggregate spacing) and taking S_{mn} as constants one can write

$$\begin{aligned} k_C^{(J)} &\propto \frac{1}{N}\int_0^N \mathrm{d}x_1 \int_0^N \mathrm{d}x_2 \left[\frac{R^2 - 2a^2(x_1 - x_2)^2}{(R^2 + a^2(x_1 - x_2)^2)^{5/2}}\right]^2 \\ &= \frac{2}{N}\int_0^N \mathrm{d}x (N - x)\frac{(R^2 - 2a^2x^2)^2}{(R^2 + a^2x^2)^5} \\ &= \frac{27}{64}\frac{1}{aR^5}\arctan\left(\frac{Na}{R}\right) + \frac{11}{64}\frac{N}{R^4(N^2a^2 + R^2)} \\ &\quad + \frac{1}{32}\frac{N}{R^2(N^2a^2 + R^2)^2} + \frac{3}{8}\frac{N}{(N^2a^2 + R^2)^3} \end{aligned} \tag{4}$$

While the above result is complicated, it reduces to simple classical results in the two opposite limits as follows:

$$k_C^{(J)} \propto \begin{cases} \dfrac{27\pi}{128a}\dfrac{1}{R^5}, & R \ll Na \\ \dfrac{N}{R^6}, & R \gg Na \end{cases} \tag{5}$$

Upon inspection of the above results, a few rationalizations are drawn. First of all, in the far-field limit where the separation is much larger than the length of the aggregates, the well-known R^{-6} dependence is recovered, while in the opposite, near-field limit the rate scales as R^{-5}, reflecting the one-dimensional geometry. Second, the factor of N in the far-field result comes from the number of acceptors, whereas there is no N dependence in the near-field limit. This results from the fact that we are essentially looking at the dipolar interaction (squared) between a monomer and a one-dimensional chain of dipoles, which is really a result of classical electrostatics.

Similarly, one finds the results for perfect H-aggregates as

$$k_C^{(H)} \propto \begin{cases} \dfrac{123\pi}{128a}\dfrac{1}{R^5}, & R \ll Na \\ \dfrac{4N}{R^6}, & R \gg Na \end{cases} \tag{6}$$

These results serve as our guideline for the quantum calculation of the EET rates, which in the high temperature limit should reduce to the former.

QUANTUM FRET: SUM OVER DIPOLES

The starting point of our investigation of the EET rates between chromophoric aggregates is the multichromophoric FRET rate in the secular approximation,

$$k_Q = \frac{2\pi}{\hbar}\sum_{\mu=1}^{N_D}\sum_{\nu=1}^{N_A}\left|\sum_{m=1}^{N_D}\sum_{n=1}^{N_A} J_{mn}C_\mu^m C_\nu^{n*}\right|^2 S_{\mu\nu}\rho_\mu \tag{7}$$

$$= \frac{2\pi}{\hbar}\sum_{\mu=1}^{N_D}\sum_{\nu=1}^{N_A}\left|J_{\mu\nu}\right|^2 S_{\mu\nu}\rho_\mu \tag{8}$$

which is obtained by approximating the donor emission and the acceptor absorption spectra being diagonal in the exciton basis.[7] C_μ^m is the wave function amplitude of exciton state μ on site m. $J_{\mu\nu}$ and $S_{\mu\nu}$ refer to the electronic coupling and the line shape overlap matrix elements in the exciton basis, respectively. ρ_μ is the probability density distribution of the donor. We adopt the convention where Roman letters represent dummy indices in the site basis while Greek letters are reserved for those in the exciton basis.

At high temperatures, the line shape overlap $S_{\mu\nu}$ can be treated as unity. In other words, the homogeneous line width is broader than the exciton bandwidth. Thus, by expanding the absolute square in eq 7, one can show that the MC-FRET expression reduces to the classical FRET expression as follows.

$$\begin{aligned} k_Q &\approx \sum_{m,m'=1}^{N_D}\sum_{n,n'=1}^{N_A}\left(\sum_{\mu=1}^{N_D} C_m^\mu \rho_\mu C_{m'}^{\mu*}\right)\left(\sum_{\nu=1}^{N_A} C_n^\nu C_{n'}^{\nu*}\right)J_{mn}J_{m'n'} \\ &= \sum_{m,m'=1}^{N_D}\sum_{n,n'=1}^{N_A}\rho_{mm'}\delta_{nn}J_{mn}J_{m'n'} \\ &= \mathrm{Tr}\rho|J|^2 = k_C \end{aligned} \tag{9}$$

We now analyze the actual quantum expression in more detail. For long linear chromophoric chains intended in this study, neglecting disorder, the exciton states are given by the Bloch states $|\mu\rangle = (1/\sqrt{N})\Sigma_m \exp(2\pi i\mu m/N)|m\rangle$. This is true as long as the intra-aggregate Hamiltonians H_D and H_A commute with the translational symmetry of the system. In this basis the coupling matrix is diagonal $J_{\mu\nu} = \delta_{\mu\nu}J_{\mu\mu}$[15] regardless of the type of aggregates (J- or H-). In the following we will focus on the calculation of $J_{\mu\mu}$ for both perfect J- and H-aggregates. In the continuum limit, this is equivalent to the evaluation of the integrals

$$J_{\mu\mu}^{(J)} = \frac{2}{N}\int_0^N \mathrm{d}x (N - x)\frac{R^2 - 2a^2x^2}{(R^2 + a^2x^2)^{5/2}}\cos\left(\frac{2\pi\mu x}{N}\right) \tag{10}$$

and

$$J_{\mu\mu}^{(H)} = \frac{2}{N}\int_0^N \mathrm{d}x (N - x)\frac{a^2x^2 - 2R^2}{(R^2 + a^2x^2)^{5/2}}\cos\left(\frac{2\pi\mu x}{N}\right) \tag{11}$$

$J_{\mu\mu}$ with $\mu = 0$. For the case of $\mu = 0$, the integrals can be carried out straightforwardly.

$$J_{\mu=0}^{(J)} = \frac{2}{Na^2}\left(\frac{1}{R} - \frac{1}{\sqrt{R^2 + N^2a^2}}\right) = \begin{cases} \dfrac{2}{Na^2R}, & R \ll Na \\ \dfrac{N}{R^3}, & R \gg Na \end{cases} \tag{12}$$

which has been obtained previously.[26,27] Here we will iterate its significance and physical interpretation, in conjunction with our

dx.doi.org/10.1021/jp4124502 | J. Phys. Chem. B 2014, 118, 7827−7834

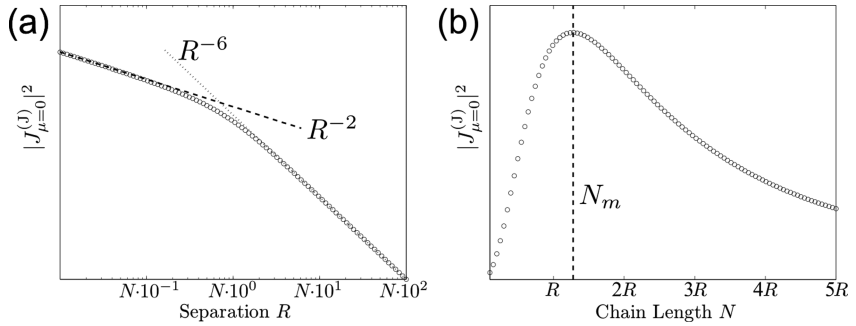

Figure 2. R and N dependence of $|J^{(J)}_{\mu=0}|^2$. (a) R dependence, both axes are in log scale. In accordance to the asymptotic limits shown in eq 12, the quantity scales as R^{-2} and as R^{-6} in the near- and the far-field limits, respectively. (b) N dependence, both axes are in linear scale. The square coupling diminishes at both ends of the N axis and reaches a maximum at $N = N_m$ given R.

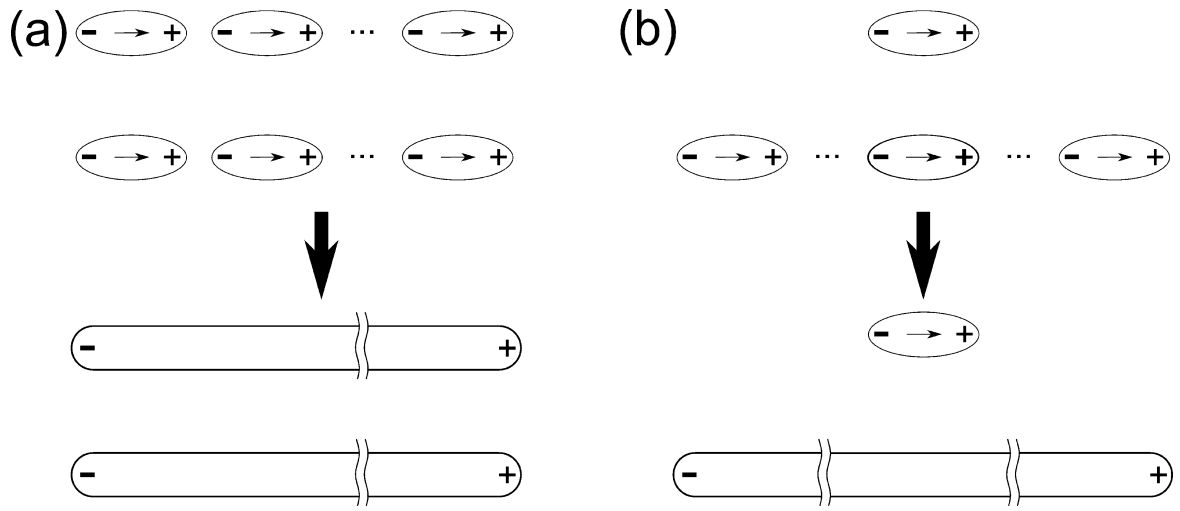

Figure 3. Schematic illustrations of effective interaction between the exciton ground states of different geometries. (a) Effective interactions between linear aggregates. (b) Effective interactions between a single chromophore and a linear aggregate.

$\mu \neq 0$ results discussed below, for a comprehensive understanding (see Figure 2). The R dependence is drawn in part a, with the near- and the far-field limits indicated in dashed and dotted lines, respectively. While the far-field result $R \gg Na$ indeed corresponds to the classical R^{-3} scaling in eq 5, the near-field limit is particularly interesting. The R^{-1} scaling can be rationalized as the destructive interference between contributions from adjacent monomers,[13,14] leaving only the couplings between monopoles at the both ends. This is valid in the regime where $Na \gg R > a$, and is shown schematically in Figure 3a. Through the successive cancellation of contributions from adjacent, opposite charges, we are left with the interactions among the ones at the very tails of the chains, which obey the R^{-1} dependence of monopolar field.

Another interesting point worth noting is the N dependence of the above expressions in eq 12, as shown in Figure 2b. It is evident that in the far-field limit the coupling is simply proportional to N. However, the inverse proportionality in the near-field limit can be understood from the argument of the effective monopole interactions made in the previous paragraph, in combination with the fact that the monopole charges scale inversely proportional to the square root of N, owing to the amplitude of the wave function on each site. The opposite dependence on N in the two limits implies an optimal coherence length which can be obtained from maximizing eq 12:

$$N_{\max} = \sqrt{\frac{1+\sqrt{5}}{2}}\frac{R}{a} \approx 1.27\frac{R}{a} \tag{13}$$

where one obtains maximal coupling. We acknowledge that this result was adopted from eq 33 of ref 23 included here for the completeness of our discussion. This is also a manifestation of the quantum interference among different donor−acceptor pairs, since classically one expects a linear dependence on system size regardless of the ratio between Na and R. This agrees with the results of Brédas et al.,[22] who quantitatively studied the R and N dependence of the exciton coupling between close-lying polyacetylene molecules in a similar scheme, in line with the earlier work of Spano and coworkers.[25]

Rossky et al., using semiempirical Pariser−Parr−Pople Hamiltonian on the level of single configuration interaction, have calculated the EET rate between tetraphenylporphyrin and oligofluorene.[24] In this case, the system resembles a monomer interacting with a linear chain of chromophores. They showed that the R dependence of the rate becomes weaker as R reduces, and reaches R^{-2} at the nearest distances allowed by steric hindrance. With minor modification of our result, it can be shown that the coupling $\overline{J}^{(J)}_{\mu=0}$ of the totally symmetric exciton state with the monomer at distance R equals

dx.doi.org/10.1021/jp4124502 | J. Phys. Chem. B 2014, 118, 7827−7834

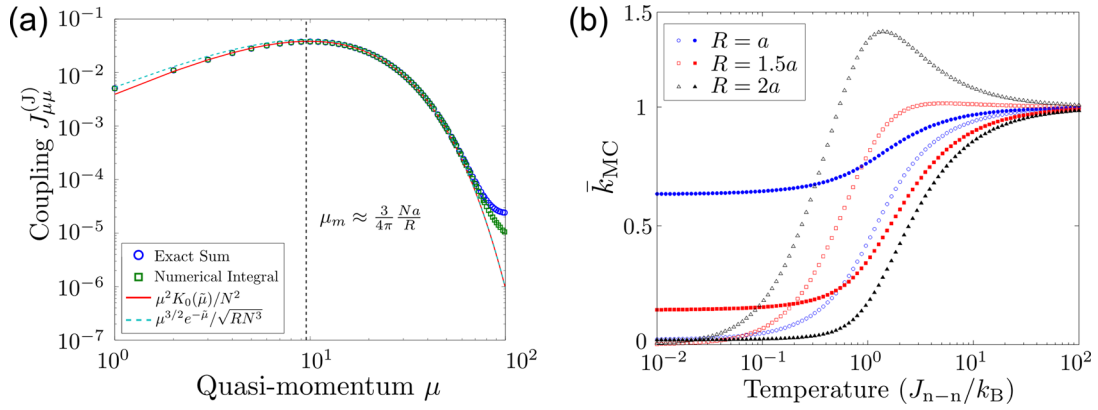

Figure 4. (a) Dependence of the inter-aggregate coupling on the exciton state label μ (quasi-momentum). Here only the case for J-aggregates $J^{(J)}_{\mu\mu}$ is shown. The results from the exact summation of eq 8 (blue circles), the numerical integration of eq 10 (green squares), and the analytical expressions eq 16 (red line) and 18 (cyan dashed line). The maximum happens at $\mu_m \approx 3Na/4\pi R$. We have taken $N = 200$ and $R = 5a$. Only half of the first Brillouin zone is plotted since $J_{\mu\mu}$ is symmetric with respect to $\mu = 0$. (b) The temperature dependence of the overall transfer rates calculated through Boltzmann averaging over all states. Open markers refer to those of the perfect J-aggregates, and filled ones denote the perfect H-aggregates. The rates are normalized to their values at infinite temperature, where all states contribute equally. The temperature is in units of the nearest-neighbor intra-aggregate coupling J_{n-n} over Boltzmann constant k_B. Circles, squares, and triangles represent the rates when the inter-aggregate separation R is equal to 1, 1.5, and 2 times of the intra-aggregate spacing a, respectively. In this figure, the aggregate size N is set to 100.

$$\bar{J}^{(J)}_{\mu=0} = \frac{8\sqrt{N}}{(4R^2 + N^2a^2)^{3/2}} = \begin{cases} \dfrac{8}{N^{5/2}a^3}, & R \ll Na \\ \sqrt{\dfrac{64N}{N^6a^6 + 12R^2N^4a^4}} \approx \dfrac{4}{\sqrt{3}N^{3/2}a^2R}, & R \approx Na \\ \dfrac{\sqrt{N}}{R^3}, & R \gg Na \end{cases} \tag{14}$$

which indeed shows no dependence on R in the near-field limit and an R^{-1} one in the small-intermediate R regime. This can also be understood through a similar argument of destructive quantum interference, as shown in Figure 3b. Here the monomer feels an effective, nearly uniform field created by the opposite charges at the ends of the chain. As such, one obtains the independence on R when $R \ll Na$. Similar to the case of parallel 1D chains as discussed earlier, there is also a nonmonotonic N dependence, and an optimal chain length is given by

$$\bar{N}_{max} = \frac{2R}{\sqrt{5}\,a} \approx 0.89\frac{R}{a} \tag{15}$$

We note that there is a recent experimental study considering an artificial system comprises chromophoric molecules intercalated onto linear DNA scaffold, which is covalently bonded to a porphyrin acceptor anchored on lipid vesicles.[29] The authors found enhanced absorption of the whole complex comparing to the direct excitation of the porphyrin due to the antenna effect. Our analysis above can be applied directly to this system, that given the monomer-chain separation one can determine an optimal chain length that maximizes the EET rate.

***$J_{\mu\mu}$* with *$\mu \neq 0$*.** To obtain closed expressions for $J_{\mu\mu}$ in general, additional assumptions need to be made. Explicitly, we drop the $-x$ in the parentheses and extend the upper limit of integration to infinity in eqs 10 and 11. In doing so we essentially assume the long chain limit, and the following expressions can be obtained:

$$J^{(J)}_{\mu\mu} \approx \frac{8\pi^2\mu^2}{N^2a^3}K_0(\tilde{\mu}) \tag{16}$$

and

$$J^{(H)}_{\mu\mu} \approx -\frac{4\pi^2\mu^2}{N^2a^3}[K_0(\tilde{\mu}) + K_2(\tilde{\mu})] \tag{17}$$

where K_α is the modified Bessel function of the second kind and $\tilde{\mu} = 2\pi|\mu|R/Na$. These are the main results of the current study. Taking the long chain limit of eq 12, one obtains vanishing $J^{(J)}_{\mu=0}$, which agrees with the above expression and can be attributed to the fact that K_0 diverges logarithmically at the origin. However, $K_\alpha(z)$ with $\alpha > 0$ diverges as $z^{-\alpha}$, thus $J^{(H)}_{\mu=0}$ has a finite value. On the other hand, in the $R \gg Na$ limit, the above expressions reduce to a delta function at $\mu = 0$, which is the correct far-field selection rule. This correctness arises from the fact that the seemingly contradicting application of the long chain limit and then the $R \gg Na$ limit does not spoil the μ dependence qualitatively. Thus, the strength of the selection rule is easily seen as a function of R with eq 16.

For a more intuitive physical picture, we make use of the asymptotic form of the Bessel function $K_\alpha(Z) \approx (\pi/2z)^{1/2}\exp(-z)$ and obtain

$$|J_{\mu\mu}| = \frac{4\pi^2}{\sqrt{a^5R}}\left(\frac{|\mu|}{N}\right)^{3/2}e^{-2\pi|\mu|R/Na} \tag{18}$$

which indicates a polynomial μ dependence with exponential cutoff, with the maximal value occurs at $\mu_{max} = 3Na/4\pi R$. It is worth noting that since we retain only the zeroth order term in the asymptotic expansion, eq 18 works for both the perfect J- and H-aggregates. However the K_2 term in the H-aggregates case decays much faster than K_0. Consequently, the true peak value of $J^{(H)}_{\mu\mu}$ occurs at $\mu \ll N$, i.e., the major contribution to the EET rate comes from the $\mu = 0$ state, which is the highest lying state for H-aggregates.

dx.doi.org/10.1021/jp4124502 | J. Phys. Chem. B 2014, 118, 7827−7834

The feature of a maximal coupling at a finite quasi-momentum $\mu = \mu_{max}$ is especially prominent when the inter-aggregate separation R is comparable to the intra-aggregate spacing a (see Figure 4a for illustration). Here we present the results from the exact sum of $J^{(J)}_{\mu\mu}$, the numerical integration of eq 10, and its continuum approximated expressions eq 16 and 18. The approximations invoked in obtaining the closed expressions are validated by the close match of these results. We note that in the limit of $\mu \to N/2$, the above-mentioned results trifurcate due to the difference between the exact summation and numerical integration, and the error originating from dropping the $-x$ term in eq 10. This is similar to the 2D case investigated by Emelianova et al.,[10] which leads to the possibility of tuning the exciton hopping rate as a function of temperature, given a particular system geometry.

Along the same line, we also present here the temperature dependence of the total transfer rates at several different separations R as shown in Figure 4b. The eigenenergies of the aggregates are obtained by assuming all intra-aggregate interactions to be dipolar. Here we neglect the contribution from the spectral overlap between the donor and the acceptor, and compute the EET rate purely on the basis of Boltzmann averaging over all states. Regardless of R, the EET rate between perfect H-aggregates is always a monotonically increasing function of temperature, as the only contributing states are at the top of the exciton band. On the other hand, the perfect J-aggregate case shows more interesting behavior. The rate shows a peak value at around $T_m \approx J_{n-n}/k_B$ for $R > a$ cases. This is attributed to the interplay between the thermal population of the exciton band (see ref 30 for details) and the functional form of $J^{(J)}_{\mu\mu}$. At low temperatures, none of the contributing states is occupied and the EET is suppressed. The rate rises at moderate temperatures and reaches the peak value when there is significant overlap between the Boltzmann distribution and $J^{(J)}_{\mu\mu}$, and then decays at higher temperatures due to the population spread to higher-lying noncontributing states.

We note that very similar nonmonotonic behavior has been observed previously through the model study on the HJ-aggregates by Spano et al.[31] They found peaked radiative decay rates of stacked conjugated polymer dimers at temperatures where $k_BT \approx J_{inter}$ (J_{inter} denotes the interpolymer excitonic coupling). We remark that not only the EET rates but also other spectroscopic properties of this interesting system setup show rich physics. This has implications on how we can design and control the energy migration pathways in low dimensional systems such as dye aggregates and thin films.[12,13,18−21]

Lastly, in the high temperature limit where all states in the exciton band are equally populated, the average EET rate should recover the classical FRET result. This is demonstrated as follows:

$$\frac{1}{N}\sum_{\mu}|J^{(J)}_{\mu\mu}|^2 \approx \frac{2}{N}\int_0^{\infty} d\mu\left[\frac{8\pi^2\mu^2}{N^2a^3}K_0\left(\frac{2\pi|\mu|R}{Na}\right)\right]^2 = \frac{27\pi}{128a}\frac{1}{R^5} \quad (19)$$

which coincides with the result in eq 5, as predicted by eq 9. The same argument applies to the perfect H-aggregates case as well.

CONCLUSION

In summary, we have studied systematically the EET rates between two parallel one-dimensional chromophore aggregates. Assuming the electronic couplings between individual pairs of chromophores to be dipolar, we first looked at the results predicted by the classical Förster theory which assumes independent hopping events among donor/acceptor pairs. However, when there is significant intra-aggregate coupling and at lower temperatures, the delocalized nature of Frenkel excitons gives rise to novel phenomena which deviates from the classical result. In this case, one inevitably needs to take into account the delocalized quantum nature of excitons. The recovery of the classical expression from the quantum one in the high temperature limit was verified and discussed. We have derived analytical expressions for the EET rates which we have used to explain the results of several preceding investigations in the literature. The results for perfect J-aggregates, where all dipoles lie in parallel to the axis of aggregation, are particularly pertinent to the photophysics of conjugated polymers. The breakdown of the far-field selection rule when the separation is comparable to or even smaller than the exciton size can be easily seen with the analytical expressions. Moreover, a nonmonotonic temperature dependence of EET rates with a maximum at moderate temperature regime is predicted, where the thermal energy is on the order of the intra-aggregate couplings. Accordingly, our results can be applied to the design principle of artificial light-harvesting devices where directional EET is preferred. Depending on situations, the geometric arrangement of molecules or temperature can be tuned to either enhance or suppress the EET along the direction of interest.

APPENDIX

Perfect H-Aggregates: Another Possibility

In the main text we have explained only one of the two possible relative orientations for perfect H-aggregates. Explicitly, the configuration with all dipoles lying within the plane of the pair of the chains was chosen. There is another possibility with all dipoles pointing outward (or inward) of this plane. In other words, the second case is obtained by rotating the dipoles ninety degrees with respect to the axes of aggregation (see Figure 5a). The dipolar interaction between such two perfect H-aggregates has a particularly simple form:

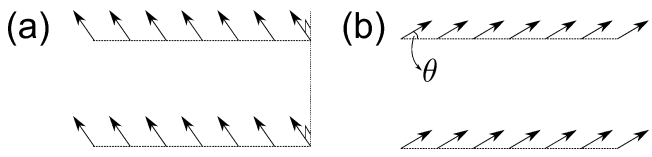

Figure 5. Additional system geometries considered in the Appendix. (a) A pair of perfect H-aggregates with their dipole orientations turned perpendicular to the plane of the aggregates. (b) General 1D linear aggregates with slanted dipole orientations, making an angle θ with the axis of aggregation.

$$J^{(H)}_{mn}\left(\frac{\pi}{2},\frac{\pi}{2}\right) = \frac{1}{r^3_{mn}} \quad (20)$$

where the arguments in the expression $J^{(H)}(\phi_1,\phi_2)$ represent the azimuthal angles of the two aggregates, so that the case

dx.doi.org/10.1021/jp4124502 | J. Phys. Chem. B 2014, 118, 7827−7834

discussed in the main text is denoted as $J^{(H)}(0,0)$. In the Bloch basis the coupling becomes

$$J_{\mu\nu}^{(H)}\left(\frac{\pi}{2}, \frac{\pi}{2}\right) = \delta_{\mu\nu}\frac{4\pi|\mu|}{Na^2R}K_1(\tilde{\mu}) \tag{21}$$

In the high temperature limit, the even averaging over all states of the above result reduces to the classical value of $3\pi/8aR^5$.

We note that the cross term $J^{(H)}(0,\pi/2)$ vanishes. As a consequence, the electronic coulping between perfect H-aggregates with arbitrary configuration (ϕ_1,ϕ_2) can be written as

$$J^{(H)}(\phi_1, \phi_2) = \cos\phi_1\cos\phi_2 J^{(H)}(0, 0) + \sin\phi_1\sin\phi_2 J^{(H)}\left(\frac{\pi}{2}, \frac{\pi}{2}\right) \tag{22}$$

This works in both site and Bloch basis, except that there is an additional diagonal selection rule in the latter.

Slanted Dipoles

Generically speaking, the dipoles constituting realistic aggregates make an angle θ with the aggregation axis as shown in Figure 5b. Then both the components of perfect J-aggregates and H-aggregates contribute to the couplings and, consequently, the EET rate. In addition to the above "diagonal terms", the cross term $J^{(M)}$ between a J- and an H-configuration also becomes non-negligible as θ is neither close to zero nor ninety degrees. It takes the following form,

$$J_{mn}^{(M)} = -3\frac{aR(m-n)}{r_{mn}^5} \tag{23}$$

or in the Bloch basis,

$$J_{\mu\nu}^{(M)} = -\delta_{\mu\nu}\frac{8\pi^2 i}{N^2a^3}\mu^2 K_1(\tilde{\mu}) \tag{24}$$

which is purely imaginary.

Noting that the above mentioned $J^{(H)}(\pi/2,\pi/2)$ does not contribute to the mix term, the most general form of the coupling between 1D aggregates can be expressed as

$$J(\theta, \phi_1, \phi_2) = \cos^2\theta J^{(J)} + \sin^2\theta J^{(H)}(\phi_1, \phi_2) + \sin\theta\cos\theta J^{(M)}(\cos\phi_1 + \cos\phi_2) \tag{25}$$

AUTHOR INFORMATION

Corresponding Author

*E-mail: jianshu@mit.edu.

Notes

The authors declare no competing financial interest.

ACKNOWLEDGMENTS

This work has been supported by the Center for Excitonics, an Energy Frontier Research Center funded by the U.S. Department of Energy, Office of Basic Energy Sciences, under Award Number DE-SC0001088 (MIT). C.C. is partly supported by the National Science Foundation (Grant Number 6924054). J.K. received support from NanoNexNL, a micro- and nanotechnology consortium of the Government of The Netherlands and 130 partners.

REFERENCES

(1) Förster, T. Zwischenmolekulare Energiewanderung und Fluoreszenz (Intermolecular Energy Migration and Fluorescence). *Ann. Phys.* **1948**, *437*, 55−75.

(2) Scholes, G. Long-Range Resonance Eergy Transfer in Molecular Systems. *Annu. Rev. Phys. Chem.* **2003**, *54*, 57−87.

(3) Wu, P. G.; Brand, L. Resonance Energy Transfer: Methods and Applications. *Anal. Biochem.* **1994**, *218*, 1−13.

(4) Silvius, J. R.; Nabi, I. R. Fluorescence-Quenching and Resonance Energy Transfer Studies of Lipid Microdomains in Model and Biological Membranes. *Mol. Membr. Biol.* **2006**, *23*, 5−16.

(5) Periasamy, A. Fluorescence Resonance Energy Transfer Microscopy: A Mini Review. *J. Biomed. Opt.* **2001**, *6*, 287−291.

(6) Clegg, R. M. F. Förster resonance energy transfer - FRET. In *FRET and FILM Techniques*; Gadella, T. W. J., Ed.; Elsevier: Oxford, 2009.

(7) Sumi, H. Theory on Rates of Excitation-Energy Transfer between Molecular Aggregates through Distributed Transition Dipoles with Application to the Antenna System in Bacterial Photosynthesis. *J. Phys. Chem. B* **1999**, *103*, 252−260.

(8) Didraga, C.; Pugzlys, A.; Hania, R.; von Berlepsch, H.; Duppen, K.; Knoester, J. Structure, Spectroscopy, and Microscopic Model of Tubular Carbocyanine Dye Aggregates. *J. Phys. Chem. B* **2004**, *108*, 14976.

(9) Ma, J.; Cao, J. Förster Resonance Energy Transfer, Absorption and Emission Spectra in Mul-tichromophoric Systems: I. Cumulant Expansions. To be submitted for publication, 2014.

(10) Emelianova, E.; Athanasopoulos, S.; Silbey, R. J.; Beljonne, D. 2D Excitons as Primary Energy Carriers in Organic Crystals: The Case of Oligoacenes. *Phys. Rev. Lett.* **2010**, *104*, 206405.

(11) Kuhn, H. Classical Aspects of Energy Transfer in Molecular Systems. *J. Chem. Phys.* **1970**, *53*, 101.

(12) Wu, J.; Liu, F.; Shen, Y.; Cao, J.; Silbey, R. J. Efficient Energy Transfer in Light-Harvesting Systems, I: Optimal Temperature, Reorganization Energy and Spatial-Temporal Correlations. *New J. Phys.* **2010**, *12*, 105012.

(13) Cao, J.; Silbey, R. J. Optimization of Exciton Trapping in Energy Transfer Processes. *J. Phys. Chem. A* **2009**, *113*, 13825.

(14) Wu, J.; Silbey, R. J.; Cao, J. Generic Mechanism of Optimal Energy Transfer Efficiency: A Scaling Theory of the Mean First-Passage Time in Exciton Systems. *Phys. Rev. Lett.* **2013**, *110*, 200402.

(15) Didraga, C.; Malyshev, V. A.; Knoester, J. Excitation Energy Transfer between Closely Spaced Multichromophoric Systems: Effects of Band Mixing and Intraband Relaxation. *J. Phys. Chem. B* **2006**, *110*, 18818.

(16) Kim, B.-G.; Jeong, E. J.; Chung, J. W.; Seo, S.; Koo, B.; Kim, J. A Molecular Design Principle of Lyotropic Liquid-Crystalline Conjugated Polymers with Directed Alignment Capability for Plastic Electronics. *Nat. Mater.* **2013**, *12*, 659.

(17) Diao, Y.; Tee, B. C.-K.; Giri, G.; Xu, J.; Kim, D. H.; Becerril, H. A.; Stoltenberg, R. M.; Lee, T. H.; Xue, G.; Mannsfeld, S. C. B.; et al. Solution Coating of Large-Area Organic Semiconductor Thin Films with Aligned Single-Crystalline Domains. *Nat. Mater.* **2013**, *12*, 665.

(18) Siebbeles, L. D. A.; Huijser, A.; Savenije, T. J. Effects of Molecular Organization on Exciton Diffusion in Thin Films of Bioinspired Light-Harvesting Molecules. *J. Mater. Chem.* **2009**, *19*, 6067−6072.

(19) Yatskou, M. M.; Donker, H.; Novikov, E. G.; Koehorst, R. B. M.; van Hoek, A.; Apanasovich, V. V.; Schaafsma, T. J. Nonisotropic Excitation Energy Transport in Organized Molecular Systems: Monte Carlo Simulation-Based Analysis of Fluorescence and Fluorescence Anisotropy Decay. *J. Phys. Chem. A* **2001**, *105*, 9498−9508.

(20) Donker, H.; van Hoek, A.; van Schaik, W.; Koehorst, R. B. M.; Yatskou, M. M.; Schaafsma, T. J. Spectroscopy and Photophysics of Self-Organized Zinc Porphyrin Nanolayers. 2. Transport Properties of Singlet Excitation. *J. Phys. Chem. B* **2005**, *109*, 17038−17046.

(21) Huijser, A.; Suijkerbuijk, B. M. J. M.; Klein Gebbink, R. J. M.; Savenije, T. J.; Siebbeles, L. D. A. Efficient Exciton Transport in Layers

of Self-Assembled Porphyrin Derivatives. *J. Am. Chem. Soc.* **2008**, *130*, 2485−2492.
(22) Beljonne, D.; Cornil, J.; Silbey, R.; Millié, P.; Brédas, J. L. Interchain Interactions in Conjugated Materials: The Exciton Model Versus the Supermolecular Approach. *J. Chem. Phys.* **2000**, *112*, 4749.
(23) Beenken, W. J. D.; Pullerits, T. Excitonic Coupling in Polythiophenes: Comparison of Different Calculation Methods. *J. Chem. Phys.* **2004**, *120*, 2490.
(24) Wong, K. F.; Bagchi, B.; Rossky, P. J. Distance and Orientation Dependence of Excitation Transfer Rates in Conjugated Systems: Beyond the Förster Theory. *J. Phys. Chem. A* **2004**, *108*, 5752.
(25) McIntire, M. J.; Manas, E. S.; Spano, F. C. Spontaneous Emission and Absorption in Model Aggregates of π-Conjugated Oligomers. *J. Chem. Phys.* **1997**, *107*, 8152.
(26) Barford, W. Exciton Transfer Integrals between Polymer Chains. *J. Chem. Phys.* **2007**, *126*, 134905.
(27) Barford, W. Beyond Förster Resonance Energy Transfer in Linear Nanoscale Systems. *J. Phys. Chem. A* **2010**, *114*, 11842.
(28) The entity S_{mn} should not be confused with the overlap integral of the donor emission and the acceptor absorption spectra, which contain the information of oscillator strengths of respective species. It is of the unit of inverse energy. See the discussion in ref 2 and ref 24.
(29) Woller, J. G.; Hannestad, J. K.; Albinsson, B. Self-Assembled Nanoscale DNAPorphyrin Complex for Artificial Light Harvesting. *J. Am. Chem. Soc.* **2013**, *135*, 2759−2768.
(30) Malyshev, V.; Moreno, P. Hidden Structure of the Low-Energy Spectrum of a One-Dimensional Localized Frenkel Exciton. *Phys. Rev. B* **1995**, *51*, 14587−14593.
(31) Yamagata, H.; Spano, F. C. Interplay between Intrachain and Interchain Interactions in Semiconducting Polymer Assemblies: The HJ-Aggregate Model. *J. Chem. Phys.* **2012**, *136*, 184901.